Author/s:
Zhang, L;Li, G;Wang, M;Di, D;Sun, L;Kronzucker, HJ;Shi, W

Title:
Excess iron stress reduces root tip zone growth through nitric oxide-mediated repression of potassium homeostasis in Arabidopsis

Date:
2018-07-01

Citation:
Zhang, L., Li, G., Wang, M., Di, D., Sun, L., Kronzucker, H. J. & Shi, W. (2018). Excess iron stress reduces root tip zone growth through nitric oxide-mediated repression of potassium homeostasis in Arabidopsis. New Phytologist, 219 (1), pp.259-274. https://doi.org/10.1111/nph.15157.

Persistent Link:
https://hdl.handle.net/11343/283842

Article type : MS - Regular Manuscript

Excess iron stress reduces root tip zone growth through nitric oxide-mediated repression of potassium homeostasis in *Arabidopsis*

Lin Zhang[1,2]*, Guangjie Li[1]*, Meng Wang[1], Dongwei Di[1], Li Sun[1], Herbert J. Kronzucker[3] and Weiming Shi[1]

[1]State Key Laboratory of Soil and Sustainable Agriculture, Institute of Soil Science, Chinese Academy of Sciences, No.71 East Beijing Road, Nanjing 210008; [2]University of the Chinese Academy of Sciences, No.19(A) Yuquan Road, Shijingshan District, Beijing 100049, China; [3]School of BioSciences, The University of Melbourne, Parkville, VIC 3010, Australia

Authors for correspondence:
Guangjie Li
Tel: +86 02586881578
Email: gjli@issas.ac.cn

Weiming Shi
Tel: +86 02586881566
Email: wmshi@issas.ac.cn

Received: *15 January 2018*

Accepted: *9 March 2018*

*These authors contributed equally to this work.

Summary

- The root tip zone is regarded as the principal action site for iron (Fe) toxicity and is more sensitive than other root zones, but the mechanism underpinning this remains largely unknown.
- We explored the mechanism underpinning the higher sensitivity at the *Arabidopsis* root tip and elucidated nitric oxide (NO)'s role using NO-related mutants and pharmacological methods.
- Higher Fe sensitivity of the root tip is associated with reduced potassium (K^+) retention. NO in root tips is increased significantly above levels elsewhere in the root and is involved in arresting primary root-tip-zone growth under excess Fe, at least in part related to NO-induced K^+ loss via *SNO1* (*sensitive to nitric oxide 1*)*/SOS4* (*salt overly sensitive 4*) and reduced root-tip-zone cell viability. Moreover, ethylene can antagonize excess-Fe-inhibited root growth and K^+ efflux, in part by controlling root-tip NO levels.
- We conclude that excess Fe attenuates root growth by effecting an increase in root-tip-zone NO, and that this attenuation is related to NO-mediated alterations in K^+ homeostasis partly via *SNO1/SOS4*.

Key words: *Arabidopsis*, Fe excess, K^+ efflux, K^+ homeostasis, nitric oxide, primary root growth, root tip zone, *SNO1/SOS4*.

Introduction

Fe is an essential element but also toxic to plants when present at elevated levels, as frequently occurs in soils of low pH and oxygen tension (Connolly & Guerinot, 2002; Becker & Asch, 2005). Plants grown in soil containing excess Fe exhibit visible symptoms of toxicity, which include biomass reduction, root growth inhibition, iron plaques in roots, leaf bronzing, and necrosis. Although physiological and molecular responses to Fe deficiency have been well documented, plant responses to Fe toxicity and Fe-toxicity-related mechanisms have received less attention.

The root is the first organ to sense excess Fe, and Fe toxicity plays a direct role in modulating root system architecture (Onaga *et al.*, 2016; Li *et al.*, 2016b). A rapid response of root tips to their changing surroundings is crucial if root development is to proceed under adverse soil conditions. Recent studies have shown that the root tip is more sensitive to Fe than other root zones but the mechanisms underpinning this are still largely unknown (Zhang *et al.*, 2011, 2012; Li *et al.*, 2015a,b). Elucidation of the mechanisms of how root tips respond to Fe toxicity will greatly help improve our understanding of the adaption and acclimation of root system architecture to metal stresses.

Plant hormones and other molecules are important intermediary signaling compounds that function downstream of environmental stimuli. Several messenger molecules such as ethylene and reactive oxygen species (ROS) are involved in mediating Fe-excess-dependent changes in root growth. Fe excess can increase H_2O_2 production in the tip zone and arrest primary root growth (Reyt *et al.*, 2015). Meanwhile, ethylene evolution is enhanced by upregulating the expression of 1-aminocyclopropane-1-carboxylic acid synthase (ACS) genes in the root tip and can protect root growth under Fe toxicity (Li *et al.*, 2015b). Recent research has unveiled NO as one critical component in plant acclimation responses to a variety of stresses, such as cadmium (Cd), copper (Cu), and aluminum (Al) stress (Neill *et al.*, 2003; Crawford & Guo, 2005; Tian *et al.*, 2007; Peto *et al.*, 2013; Alemayehu *et al.*, 2015). Under Fe scarcity, NO increases in the root and can affect Fe uptake from the culture environment (Pagnussat *et al.*, 2002; Graziano & Lamattina, 2007). Similarly, NO production has been reported to increase under Fe overload (Arnaud *et al.*, 2006; Touraine *et al.*, 2012). Thus, it could be predicted that there may be links between NO and the Fe-toxicity response in plants. However, there has been no detailed study to evaluate the role of NO in the Fe-toxicity response in plant development, and especially not in relation to primary root growth.

A number of studies have shown that intracellular K^+ participates in many defence-related processes, and that various abiotic and biotic stresses induce K^+ efflux from root cells (Demidchik *et al.*, 2003, 2010). In most cases, this K^+ efflux is mediated by K^+-selective channels, nonselective cation channels (NSCCs), and annexins (reviewed in Demidchik, 2014). The guard cell outward-rectifying K^+ channel (GORK) *GORK1* is well known to conduct large outwardly directed K^+ currents from root cells in response to copper ascorbate and/or NaCl, and NaCl-activated K^+ efflux from roots is significantly decreased in the *gork1-1* mutant (Demidchik *et al.*, 2010; Demidchik, 2014). Nonselective cation channels belong to a variety, and as yet to be solidly identified, gene families (e.g. cyclic nucleotide gated channel (CNGC) gene families contain 20 genes in *Arabidopsis*, glutamate receptors (GLR) gene families contain 20 genes in *Arabidopsis*) form a group with a cryptic molecular identity and diverse functional characteristics (Demidchik & Maathuis, 2007; Kronzucker & Britto, 2011). The big challenge in studies of plasma-membrane-resident NSCC is the persistent lack of knowledge of the encoding genes and the fact that single loss-of-function mutations do not result in clear phenotypes (Pottosin & Dobrovinskaya, 2014). Under Fe toxicity, a significant loss in plant tissue K level has been noted (Li *et al.*, 2001, 2015b, 2016a), but the morphological and physiological mechanisms of root K^+ homeostasis under Fe excess has not been identified. A recent study showed that ethylene can maintain root K^+ status by regulating K^+ uptake to support root growth under Fe toxicity (Li *et al.*, 2015b). In addition, the possibility that NO contributes to modulate K^+ accumulation by plants has been recently advanced (Simontacchi *et al.*, 2015). The *SNO1*/*SOS4* gene encoding a pyridoxal kinase was recently identified as playing a critical role in NO-mediated root K^+ homeostasis (Shi *et al.*, 2002; Xia *et al.*, 2014). Xia *et al.* (2014) demonstrated that enhanced NO increases the accumulation of pyridoxal-5'-phosphate (PLP), which, in turn, represses K^+ uptake in *Arabidopsis* roots, and NO-triggered PLP accumulation mainly occurs through NO-induced SNO1/SOS4 enzyme activity. Although ethylene and NO signals have been implicated as important for root K^+ homeostasis, it remains largely unknown how ethylene and NO are involved in the response of root K^+ homeostasis to excess Fe.

In this study, we employed *Arabidopsis Columbia-0* (*Col-0*) and NO- and ethylene-related mutants, to explore the possible mechanism underpinning the higher sensitivity to Fe toxicity of the root tip zone, and to elucidate the roles of NO and ethylene. Potential mechanisms involved in the stress response to excess Fe are discussed.

Materials and Methods

Plant materials and growth conditions

Seedlings of the following lines were used in this study: *Arabidopsis thaliana* (L.) Heynh. ecotype *Columbia-0* (*Col-0*); the mutants *nox1*(*nitric oxide overproducer1*), *gsnor1* (*S*-nitrosoglutathione (GSNO) reductase1), *sno1/sos4*, *noa1* (NO Associated1), *pin2-1*, *pin3-5*, *tir1-1*, *pin1-1*, *axr2-1*, *axr3-3* (Arabidopsis Biological Resource Centre, Table S1), *eto2-1* and *EIN3 binding site* (*EBS*)*: b-Glucuronidase* (*GUS*), *Direct Repeat 5* (*DR5*)*: GUS*, *ACS7:GUS*, *DR5: Green Fluorescent Protein* (*GFP*) transgenic lines were in a *Col-0* background, and the *gork1* mutant was in a *Wassilewskija* (*WS*) background. Seeds were surface-sterilized and cold-treated at 4°C for 48 h before being sown on standard growth medium. The standard growth medium was as described previously (Li *et al.*, 2013), and was composed as follows: 2 mM KH_2PO_4, 5 mM $NaNO_3$, 2 mM $MgSO_4$, 1 mM $CaCl_2$, 50 μM Fe-EDTA, 50 μM H_3BO_3, 12 μM $MnSO_4$, 1 μM $ZnC1_2$, 1 μM $CuSO_4$, 0.2 μM Na_2MoO_4, 1% sucrose, 0.5 g/liter MES, and 0.8% agar (adjusted to pH 5.7 with 1 M NaOH). The day of sowing was considered day 0. Seedlings were grown, oriented vertically on the surface of the culture plates in a growth chamber, set to a 16 h : 8 h, light : dark photoperiod, an irradiance of 100 μmol·m^{-2}·s^{-1}, and a temperature of 23 ± 1°C. Excess Fe was supplied as Fe-EDTA ($FeSO_4 \cdot 7H_2O$ plus EDTA, 1:1 molar ratio).The pH was set to 5.3, based on our previous report (Li *et al.*, 2015b). To study the effect of exogenous 2-(4-carboxyphenyl)-4,4,5,5-tetramethylimidazoline-1-oxyl-3-oxide (cPTIO), sodium nitroprusside (SNP), aminoethoxyvinylglycine (AVG), NG-nitro-L-arginine methyl ester (L-NAME), NG-Monomethyl-L-arginine (L-NMME), tetraethylammonium (TEA), Gd^{3+}, and K^+ (supplied as K_2SO_4), seedlings were supplemented with varying concentrations of Fe-EDTA plus indicated concentrations of the added compounds. All chemicals were obtained from Sigma-Aldrich.

Localized Fe-supply experiments

Localized excess-Fe treatments were shown in Supporting Information Fig. S1, as described in our previous report (Li *et al.*, 2015a). Briefly: for 'root tip-supplied' plants, segmented agar plates were separated into upper and lower parts with a 3-mm air gap, using movable glass strips 3 mm in width. Growth medium was poured into the upper part, the excess Fe-EDTA medium was poured into the bottom part, and only the primary root tip of the seedlings (*c.* 2 mm) was in contact with the excess Fe-EDTA medium. For 'root-hair-zone-supplied Fe' plants, growth medium was poured into the bottom part, excess Fe-EDTA medium was poured into the upper part, and only the shoot and primary root hair zone of the seedlings were in contact with the excess Fe-EDTA medium. Treatment was for the times indicated.

Root measurements

Roots on the agar surface were sampled. The lengths of primary roots of individual seedlings were measured directly with Image J software from digital images captured with a Canon G7 camera. Primary root elongation was defined as the length of the root parts newly grown after treatment. Measurements were made of the length from the root cap to the first root hair.

Microscopy and image and mineral analysis

The Fe-specific Perls staining and diaminobenzidine (DAB) intensification was adapted from Roschzttardtz *et al.* (2009). Localization of Fe was observed and imaged using an Olympus BX51 microscope equipped with differential interference contrast (DIC) optics and an Olympus DP71 camera. Histochemical analysis of GUS reporter enzyme activity was performed as described elsewhere (Weigel & Glazebrook, 2002). Trypan Blue (TB) staining was used to assess the level of cell death in the root tips under excess Fe according to the method of Duan *et al.* (2010) with some modifications. The *DR5:GFP* reporter was analysed using a Zeiss LSM710 confocal microscope, and image analysis was performed using Zeiss 2009 software (Carl Zeiss AG, Jena, Germany). NO and ROS were visualized using the NO-specific fluorescent probe DAF-FM DA (5 μM) and the ROS fluorescent probe CM-H_2DCFDA (25 μM), respectively, according to the method of Wang *et al.* (2014) with some modifications. Asante Potassium Green-2 (APG-2, TEFLabs, Austin, TX, USA) and CoroNa Green acetoxymethyl (AM) ester (Invitrogen, Eugene, OR, USA) were employed to measure K^+ and Na^+ concentrations according to Wang *et al.* (2016). 20 μM APG-2 and CoroNa Green were added to measuring buffers, respectively (K^+: 5 mM NaCl, 5 mM Ca^{2+}-MES, pH 6.1; Na^+: 10 mM KCl, 5 mM Ca^{2+}-MES, pH 6.1) and incubated with the *Arabidopsis* seedlings for 3 h in the dark at room temperature. Fluorescence intensity of NO, APG-2, CoroNa Green, and ROS was determined by calculating the relative contribution of the green channel using the values of the RGB colour model as measured in Photoshop 7.0 (Adobe Systems), according to Teerawanichpan *et al.* (2007). All staining and image analysis procedures were repeated at least twice, and results shown are from one of two representative experiments. For mineral analyses, samples were obtained from root tip sections (*c.* 1–2 mm) from both control and excess-Fe treatments. The samples (0.5–1.0 mg) were digested with 0.25 ml of concentrated HNO_3 at 110°C for 2 h according to Ward *et al.* (2008) and analyzed on an ICP-MS (Agilent, Santa Clara, California USA).

Enzyme activity analyses of SNO1/SOS4

The activity of SNO1/SOS4 was measured using a colorimetric procedure, according to the protocols described by Xia *et al.* (2014). Briefly: 0.5 mL crude extract (containing 1–7 mg total protein) was used in a buffer containing 0.2 mM pyridoxal, 0.2 mM ATP, 0.1 mM $ZnCl_2$, and 70 mM K_3PO_4 was used. After 1 h incubation at 37 °C, reactions were stopped by 50 mL chilled 50% trichloroacetic acid (TCA) (w/v). Protein was pelleted by centrifugation (1500 ***g***) at 4°C for 10 min, and then the supernatant was transferred to a clean tube. After the addition of 2% phenylhydrazine (in 10 N H_2SO_4) and incubation on ice for 30 min, the PLP formation was measured based on the absorbance at 410 nm. Each reaction was repeated three times.

Measurement of net K^+ flux with the SIET system

Net fluxes of K^+ were measured from the root apical (*c.* 500 μm from the tip of *Col-0* roots) transition zone and the root hair (*c.* 3000 μm from the tip of *Col-0* roots) zones using non-invasively using SIET (scanning ion-selective electrode technique, SIET system BIO-003A; Younger USA Science and Technology Corp.; Applicable Electronics Inc.; Science Wares Inc., Falmouth, MA, USA). The principle of this method and the instrument are as detailed in Li *et al.* (2010) and Shabala *et al.* (2016). *Arabidopsis* seedlings were grown in a Petri dish for 7 d. For the pretreatments, plants were pretreated with mock solution and plus indicated concentrations of cPTIO, SNP, TEA, Gd^{3+}, AVG, PLP, and K^+ for 2 h. After the specified pretreatment duration, the pretreatment solution was withdrawn and the measuring solution was introduced. Net ion fluxes were first measured in the basal medium to ensure steady initial values, then 10 mM stock solution of Fe-EDTA was applied to reach a final Fe concentration of 300 μM. Transient recordings of the flux kinetics of K^+ were measured for specified times. All measurements of net K^+ fluxes were carried out at Xuyue Science and Technology Co., Ltd (Beijing, China).

Statistical and graphical analyses

For all experiments, data were statistically analyzed using the SPSS 13.0 program (SPSS Chicago, IL, USA.). Details are as presented in figure legends. Graphs were produced using Origin 8.0. All graphs and images were prepared using Adobe Photoshop 7.0.

Results

The root tip is the critical site in the arrest of *Arabidopsis* primary root growth under Fe toxicity

To analyze the effect of Fe toxicity on primary root growth, *Arabidopsis* seedlings were allowed to come into contact with varying concentrations of Fe-EDTA. Based on our previous report (Li *et al.*, 2015b), 50 μM Fe was used as a control. Increased Fe concentrations significantly inhibited primary root growth (Fig. 1a). Primary root growth was also quantified at 1, 2, and 3 d after transfer. Exposure of the seedlings to excess Fe (300 μM) resulted in an immediate arrest of root growth at indicated timing (Fig. 1b). Further results showed that Fe-excess-induced root growth inhibition required that the root tip was in direct contact with external Fe (Figs S1, 1c) and the distance from the root apex to the emergence of the first root hair under Fe toxicity was reduced to *c.* 50% of that in controls (Fig. 2a,b). These results suggest that root apical tissues are more sensitive to excess Fe and are immediately growth-arrested upon excess-Fe treatment.

To investigate whether the higher sensitivity of the root apex is associated with higher Fe accumulation than in the root hair zone, we used a sensitized, Fe-specific, histochemical procedure (Perls/DAB staining) that reports labile (non-heme) Fe^{3+} and some Fe^{2+} (Meguro *et al.*, 2007; Muller *et al.*, 2015). Under excess Fe, the intensity of the Perls-DAB was much deeper in the root hair zone compared with the tip zone (Fig. 2c). The phenomenon was also observed by the Perls method (no DAB enhancement) (Fig. S2). Thus, the arrest of root growth upon exposure of the root tip to excess Fe (Figs 1c, 2a,b) may not be explained by a higher accumulation of iron in the root tip.

Higher sensitivity of the root tip zone to Fe may be related to impaired potassium homeostasis

Potassium (K) has been reported to play a critical role in regulating root development under Fe toxicity. We, thus, analyzed changes of K^+ level in functionally different root zones (root hair zone and tip zone). Imaging using the APG2 fluorescing dye revealed that excess Fe led to a decline in the K^+ level of the root tip zone, but no significant changes were observed in the root hair zone over the times of treatment (Fig. 2d,e). Mineral analysis using ICP-MS further showed a significant decrease in the root-tip-zone potassium content under excess-Fe treatment (Fig. 2f). Analysis of root growth revealed localized K^+ deficiency in the root tip, but not in the root hair zone, enhancing the sensitivity of root growth to Fe (Fig. S3). As well, a slight decrease was found in root-tip-zone sodium (Na) staining (Fig. S4a). However, localized Na^+ deficiency in the root tip zone did not significantly enhance the sensitivity of root growth to Fe toxicity (Fig. S4b). There was no significant decrease in the root-tip-zone calcium (Ca) and magnesium (Mg) contents over the same time of excess-Fe treatment (Fig. S4c).

To examine K^+ net fluxes at the root surface in response to excess Fe in functionally different *Col-0* root zones, we used the SIET on *Arabidopsis* roots (Ludewig *et al.*, 2003). Upon excess-Fe stimulation, there was a significant efflux of intracellular K^+ in the tip zone (Fig. 3a). By contrast, the root hair zone (*c.* 3000 μm from the tip of roots) showed no remarkable changes in SIET signals under the same conditions. The mean K^+ effluxes under excess Fe were significantly different between the two root zones (Fig. 3b). As described above, Fe-inhibited root growth requires that the root tip come into contact with external Fe (Fig. 1c). It was therefore important to ask whether K^+ fluxes at the root apex may be changed by direct Fe contact. Addition of excess Fe to the whole root or only the root tip resulted in a massive K^+ efflux in the root tip zone, whereas the mean K^+ flux was similar when the whole root or only the root tip zone was exposed to excess Fe (Fig. 3c,d). When excess Fe was not supplied to the root tip, there were no significant changes in SIET signals in the root tip zone (Fig. 3c,d).

K^+-selective channels and NSCCs are documented to be involved in K^+ efflux from roots (Coskun *et al.*, 2010; Kronzucker & Britto, 2011; Demidchik, 2014; Shabala *et al.*, 2016). To delineate between those channels, exogenous TEA, a well-known inhibitor of K^+-channel activity (Coskun *et al.*, 2010, 2013b), and Gd^{3+}, a known blocker of NSCCs (Kronzucker & Britto, 2011), were applied to *Arabidopsis* seedlings. Compared with the mock condition, Fe-induced K^+ efflux was similar in TEA-pretreated seedlings. However, the Gd^{3+} application significantly decreased the Fe-induced root-tip K^+ efflux (Fig. 4a,b) and mildly alleviated the decrease in the rate of root growth compared with Fe treatment alone (Fig. S5a). The outwardly rectifying K^+-channel *GORK1* is well known to conduct large K^+ effluxes in response to copper and Na (Demidchik *et al.*, 2010; Demidchik, 2014). However, mean K^+ effluxes in the root tip zone did not show significant differences between the wild type and the *gork1* mutant under excess Fe, and root growth was decreased in *gork1* to a similar extent as in the wild type (Figs 4c,d, S5b).

K^+ deficiency resulted in severe root-growth inhibition and the root-growth inhibition by excess Fe in *Col-0* was alleviated by K^+ addition (Becker & Asch, 2005; Li *et al.*, 2015b; Fig. S6a). K^+ addition led to increased tip-zone K content, but did not affect K^+ efflux at the root tip in response to excess Fe (Fig. S6b,c).

Excess Fe affects root tip zone growth through overaccumulation of NO

Fe overload stimulates NO accumulation (Arnaud *et al.*, 2006). Indeed, treatment with excess Fe resulted in significant accumulation of NO in *Arabidopsis* roots (Fig. 5a,b). However, this accumulation was more significant in the root tip zone (Fig. 5a,b).

To investigate the possible role of NO in Fe-induced inhibition of root growth, we first investigated the effects of cPTIO (a widely used NO scavenger) and SNP (an NO donor) on root growth under excess Fe. Application of cPTIO clearly reversed the decrease in the rate of primary root growth and the root tip zone size compared with Fe treatment alone (Fig. 6a,b). However, application of SNP to the root tip clearly enhanced the Fe-induced inhibition of root growth (Fig. 6c). Infiltration with either L-NAME or L-NMME (inhibitors of animal NO synthase (NOS) that is also effective in plant systems) did not significantly modify Fe-induced inhibition of primary root growth (Fig. S7a), while they have been shown to reduce the inhibitory effect of salt treatment on root growth (Liu *et al.*, 2015; Fig. S7b). Furthermore, the root growth of the *noa1* mutant, which exhibits reduced endogenous NO levels, was also similar to *Col-0* under Fe excess (Fig. S7c). This result supports the previous finding that NOS inhibitors (L-NAME and L-NMME) and the mutation in NOA1 did not significantly affect the excess-Fe-induced NO production (Touraine *et al.*, 2012).

In agreement with pharmacological studies, exposure of the NO-overproduction mutants *nox1* and *gsnor1* to excess Fe concentrations led to more inhibition of root growth than in *Col-0* (Figs 6d, S8). To ascertain that the observed primary root phenotypes were specifically due to high Fe concentrations and not to the organic chelate, similar experiments were performed using Fe-citrate instead of Fe-EDTA (Fig. S9), and *nox1* retained higher sensitivity of root growth. The spatial response to Fe was also compared between *Col-0* and *nox1*, and a difference in Fe-inhibited root growth between the two genotypes was only found when the root tips were exposed to excess Fe (Fig. 6e). In agreement with this, the size of the primary root tip zone was much more reduced in *nox1* than *Col-0* when Fe was supplied in a localized manner to the root tip (Fig. 6f). Iron excess has been documented to be associated with enhanced throughput through Fenton reactions. We also tested the response of *nox1* root growth to excess Cu that is also associated with Fenton reactions. However, *nox1* displayed increased root growth tolerance than *Col-0* under Cu excess (Fig. S10).

Auxin has been suggested to be involved in root growth under several stresses (Giehl *et al.*, 2012; Yuan *et al.*, 2013), and, thus, was examined here. Although the level of the *DR5*:*GUS* reporter gene in the root apex of *wei7-2* mutant, in which auxin biosynthesis is impaired (Yang *et al.*, 2014), was markedly reduced compared with *Col-0* (Fig. S11a,b); Fe had a similar impact on root-growth inhibition in both genotypes. Analysis of the response of auxin-transport and -signaling mutants showed that root growth was decreased in auxin transport mutants (*pin1-1*, *pin3-5*) and in signaling mutants (*tir1-1*, *axr2-1*, *axr3-3*) to a similar extent as in *Col-0*, with slight sensitivity to Fe observed in the *pin2-1* mutant. *DR5:GFP* expression was further analyzed in roots treated with excess Fe plus cPTIO. Although cPTIO co-treatment relieved the Fe-mediated inhibition of root growth, it had no effect on *DR5:GFP* expression (Fig. S11c).

Recent studies (Reyt *et al.*, 2015; Onaga *et al.*, 2016) suggested that Fe homeostasis interferes with ROS distribution in the primary root, and that this interaction may contribute to NO-mediated primary root shortening under Fe excess. Consistently, excess Fe significantly induced ROS in the root tip zone of both *Col-0* and *nox1* seedlings (Fig. S12); however, the ROS levels in *nox1* did not significantly differ from the *Col-0*.

NO contributes to excess-Fe-mediated K^+ depletion and cell death in the root tip zone

Given that excess Fe markedly induced root-tip K^+ loss (cf Figs 2, 3), we asked whether endogenous NO levels in Fe-treated plants were related to K^+ loss in root tips exposed to Fe stress. As shown in Fig. 7(a,b), the pretreatment of *Arabidopsis* roots with the NO scavenger cPTIO reduced the excess-Fe-induced *Col-0* root-tip K^+ efflux. By contrast, SNP pretreatment significantly enhanced K^+ efflux in the *Col-0* tip zone under both control and Fe treatment conditions (Figs 7a,b, S13a). Moreover, the *nox1* mutant exhibited more K^+ efflux in the root tip zone than the *Col-0* under both control and Fe-treatment conditions (Figs 7c,d, S13b,c). Gd^{3+} pretreatment reduced the Fe-induced root tip K^+ efflux in the *nox1* mutant (Fig. 7e,f). Moreover, Gd^{3+} did not affect excess-Fe-induced NO levels in the *Col-0* root tip (Fig. S14). Imaging, using the APG-2 fluorescent dye, revealed a lower K^+ level in the root-tip zone of the *nox1* mutant than in *Col-0* under Fe stress (Fig. 8).

Fe excess and NO accumulation have also been reported to trigger cell death (Bai *et al.*, 2012; Li *et al.*, 2012). In these studies, the rate of regrowth of Fe-treated roots was significantly different from the controls, although the root growth of both *Col-0* and *nox1* following treatment was largely recovered after 24 h of recovery culture. Moreover, the regrowth rate of *nox1* was lower than in *Col-0* (Fig. S15a). We further stained roots with excess Fe using TB staining (Duan *et al.*, 2010). Compared with the control, exposure to excess Fe led to increased TB staining intensity at the root tip zone, and the TB staining intensity in *nox1* was significantly higher than in *Col-0* (Fig. S15b). We also tested the effect of K^+ deficiency under excess Fe on the TB staining at the root tip zone. K^+ deficiency significantly enhanced *Col-0* root-tip-zone TB staining under Fe toxicity (Fig. S6d).

SNO1/SOS4 has been reported as a critical factor of NO modulation of K^+ levels in *Arabidopsis* roots and the activity was induced by NO (Xia *et al.*, 2014). Consistently, *SNO1/SOS4* activity was increased in SNP-treated *Col-0* seedlings, compared with controls (Fig. 9a). Also, an increase of *SNO1/SOS4* activity was observed in the Fe-treated *Col-0* and *nox1* seedlings; however, the induction was more significant in *nox1* (Fig. 9a). Moreover, compared with *Col-0* controls, the *sno1/sos4* mutant exhibited aggravated root growth inhibition and significantly more root-tip-zone K^+ efflux in response to excess Fe (Fig. 9b,c,d). The elevated PLP content directly mediated by increased *SNO1/SOS4* activity was reported to play roles in regulating K^+ currents (Xia *et al.*, 2014). In this study, the PLP pretreatment significantly enhanced excess-Fe-induced K^+ efflux in the *Col-0* root tip zone, and application of Gd^{3+} could reverse the PLP-induced K^+ efflux under excess Fe (Fig. 9e,f). Seedlings grown under K^+ addition plus cPTIO showed well developed root growth compared with K^+ addition alone (Fig. S16a). However, no significant alleviation by K^+ addition was observed in *nox1* and *sno1/sos4* mutants under Fe stress, compared with *Col-0* (Fig. S16b), even when exogenous K^+ was increased to 10 mM (data not shown).

Ethylene negatively regulates the excess-Fe-induced NO accumulation

Ethylene has been suggested to alleviate Fe toxicity in some cases. The *AtACS7* gene has been reported to play a key role in excess-Fe-induced ethylene production (Li *et al.*, 2015a,b); herein, *AtACS7:GUS* activity, in which the GUS reporter gene is driven by the *AtACS7* promoter, was markedly increased in the root tip under excess Fe (Fig. 10a). Consistent with this, the *EBS:GUS* expression (an ethylene reporter construct in which the GUS reporter gene is driven by a synthetic EIN3-responsive promoter) was also enhanced markedly in the root tip zone under Fe excess (Fig. S17). Supplementation with AVG, an inhibitor of ethylene biosynthesis, aggravated the inhibition of primary root growth under Fe excess (Fig. 10b). Meanwhile, *eto2-1*, a gain-of-function *ACS5* mutant allele of *ETO2*, which confers increased ethylene production (Wang *et al.*, 2004), displayed increased root-growth tolerance compared with *Col-0* (Fig. 10c).

As ethylene and NO are both involved in the regulation of root growth under Fe excess, their roles here needed to be determined. NO-dependent fluorescence in root tips was significantly increased in the presence of the ethylene inhibitor AVG under Fe excess (Fig. 10d). This was further supported by the observation that Fe-induced NO generation in root tips was lower in *eto2-1* than in *Col-0* (Fig. 10e). Interestingly, application of the NO donor SNP could increase the *AtACS7:GUS* expression in the root tip under excess Fe, compared with the mock condition (Fig. S18). We further examined the role of ethylene in Fe-regulated K^+ fluxes. In *Col-0* plants, AVG pretreatment significantly enhanced Fe-induced K^+ efflux in the root tip zone compared to the mock condition (Fig. 10f,g).

Discussion

Previous, and our present results, show that excess Fe supplied to *Arabidopsis* roots can regulate the distal organizer pattern in the root tip (Reyt *et al.*, 2015; Fig. 2a,b). Excess-Fe-induced root growth inhibition requires that the root tip be in direct contact with external Fe, and the root tip zone is more sensitive to Fe toxicity than other root zones (Zhang *et al.*, 2011; Li *et al.*, 2015b; Fig. 1c). However, it has remained unclear what processes underpin the higher sensitivity of the root tip to Fe stress. In our study, we found that the higher Fe sensitivity was related, at least in part, to compromise K^+ retention in the root-apical zone. Further examination revealed that the sensitivity of the root tip zone, the impairment of K^+ homeostasis in that zone, and cell death under Fe toxicity, were connected to Fe-induced NO accumulation. To assist in the interpretation of a complex data set that highlights the importance of NO accumulation and K^+ homeostasis responses to excess Fe, we provided a model to explain the growth inhibition of root-apical tissues at the molecular and physiological level (Fig. 11).

Maintaining sufficient K^+ levels enhances plant tolerance to various environmental stresses (Kronzucker *et al.*, 2008; Britto & Kronzucker, 2009; Szczerba *et al.*, 2009; Coskun *et al.*, 2010, 2013a; Li *et al.*, 2014). A strong positive correlation between the ability to retain K^+ and Fe-excess tolerance was previously reported in rice (Onaga *et al.*, 2016), *E. hirsutum* (Wheeler *et al.*, 1985) and *Arabidopsis* (Li *et al.*, 2016a). Although excess Fe was previously reported to inhibit root growth by negatively regulating K^+ homeostasis (Li *et al.*, 2001, 2015b; Çelik *et al.*, 2010), how Fe excess impacts root K^+ homeostasis has remained rather poorly understand. In our study, we found that Fe-excess-induced K^+ loss was especially pronounced in the root tip zone. Root apical zones have more K^+ efflux and retain less K^+ when exposed to Fe excess (Figs 2, 3), and K^+ deficiency in root apical zones could aggravate excess-Fe-inhibited root growth inhibition (Figs S3, S6a). Cells that are not completely differentiated, especially those in the root meristem, are characterized by a small vacuole, low volume, low water content, and low fresh weight (Luxova, 1988). Shabala *et al.* (2006) suggested that higher net K^+ efflux implies lower cytosolic K^+, which could alter cell elongation processes. K^+ efflux across the root plasma membrane is reported to be mainly mediated by GORK and NSCCs (Coskun *et al.*, 2010; Demidchik, 2014; Shabala *et al.*, 2016). Copper-ascorbate-induced K^+ loss from *Arabidopsis* roots is mediated by K^+-selective channels (K^+ loss was blocked by TEA and reduced in the *gork1* mutant) (Demidchik *et al.*, 2010). However, both TEA pretreatment and GORK1 mutation had no significant effect on the root-tip K^+

efflux under excess Fe (Fig. 4). Persistent lack of certainty around which molecular candidates are coding for NSCCs, and the lack of clear phenotypes in loss-of-function mutants, present a significant challenge in studies of NSCCs and in attempts to relate their function mechanistically to a number of physiological phenomena (Kronzucker & Britto, 2011; Pottosin & Dobrovinskaya, 2014). Pharmacological NSCC blockers, such as Gd^{3+}, which tend to display broader-spectrum inhibition (Kronzucker & Britto, 2011), are, however, widely used in studies on NSCCs; for example Zepeda-Jazo *et al.* (2011) suggested that copper-ascorbate-induced K^+ efflux from pea roots is mediated by NSCCs, by using evidence derived from Gd^{3+}. Here, a large contribution of NSCCs is suggested by the fact that Gd^{3+} caused a *c*. 60% inhibition of excess-Fe-induced K^+ efflux (Fig. 4a,b), and application of Gd^{3+} could mildly alleviate the decrease in the rate of root growth under Fe toxicity (Fig. S5a). Furthermore, our present, and previous, data show suppression of root growth under excess Fe can be significantly alleviated by K^+ addition (Li *et al.*, 2016a; Fig. S6a), and K^+ addition can lead to higher tissue K levels (Fig. S6c), supporting the importance of the role of K^+ retention in tolerance to excess Fe.

In contrast to the study of NO's roles in the response to Fe limitation, the possible roles of NO in regulating root growth under Fe surplus have not been investigated. In this study, we demonstrate that root growth effects under Fe excess are mediated, at least in part, by NO accumulation (Figs 5, 6). To cope with Fe deficiency, plants must ensure effective Fe acquisition from the rhizosphere. Iron-deficiency-induced NO can trigger the expression of the *FIT* gene, which regulates the expression of *FRO2* and *IRT*, to increase the uptake of iron (Chen *et al.*, 2010). By contrast, under excess-Fe conditions, restriction of excessive Fe absorption can prevent more serious Fe toxicity (Becker & Asch, 2005), and the expression of the *IRT1* gene is significantly inhibited at high iron concentrations (Giehl *et al.*, 2012). The function of NO in promoting iron uptake is useful in the acclimation to Fe deficiency but seems to not be conducive to improving responses to excess-Fe conditions. It is, however, not known whether NO may directly modulate root Fe influx and/or efflux under excess Fe, and more research is warranted to examine this. Other metals, such as Cu and Al, have been also shown to produce oxidative stress and inhibit root growth (Xiong *et al.*, 2010), but, in contrast to excess Fe stress, NO plays a positive role in Cu and Al toxicity tolerance in relation to root growth (Tian *et al.*, 2007; Peto *et al.*, 2013; Liu *et al.*, 2016; Fig. S10), although NO plays a negative role in Al tolerance in some plants, such as rice bean (Zhou *et al.*, 2012). Thus, it can be hypothesized that, depending on the biological context, NO exerts opposing effects on root growth. L-NAME (a NOS inhibitor) has been reported to reduce salt-induced NO production in *Arabidopsis* (Liu *et al.*, 2015), and L-NAME can reduce the inhibitory effect of salt treatment on root growth (Liu *et al.*, 2015; Fig. S7b). Chen *et al*. (2010) demonstrated that NOS and the *NOA1* gene are involved in Fe-deficiency-regulated NO generation in the *Arabidopsis* root-tip zone, and Fe-deficiency-induced NO accumulation and gene expression were significantly suppressed by the NOS-inhibitor L-NAME and by the *NOA1* mutation. By contrast, Touraine *et al.* (2012) clearly showed that treatment with L-NAME or L-NMMA and the mutation in *NOA1* do not affect Fe-excess-dependent NO production in *Arabidopsis*. Our present data show that L-NAME or L-NMME and the mutation in *NOA1* have no significant effect on excess-Fe-inhibited root growth (Fig. S7a,c), supporting the results of Touraine *et al.* (2012). All the results to date suggest that the regulatory mechanisms underpinning NO accumulation in *Arabidopsis* are fundamentally different in response to Fe deficiency as opposed to Fe excess. NO production from different sources may result in divergent effects (Xiong *et al.*, 2010), even in response to the same stress. For example, nitrate-reductase (NR)- rather than NOS- and other source-mediated NO bursts are involved in the protection against Al toxicity in roots of wheat (Sun *et al.*, 2014). At least seven possible pathways of NO biosynthesis have been described in plants (Gupta *et al.*, 2011). However, to date, the mechanisms underlying the induction of NO biosynthesis under excess Fe in plants is still largely unknown. Further studies on the precise origin of excess-Fe-induced NO in plant tissues are warranted.

The question then arises as to how Fe-induced NO accumulation leads to impaired resistance to Fe excess. It's suggested that NO can suppress root growth by reducing auxin in root tips under salt and Cd stress (Liu *et al.*, 2015; Yuan & Huang, 2016). However, unlike as in salt or Cd stress, the *DR5*-indicative auxin level in the root tip was not reduced under excess Fe, although a NO burst and inhibition of root growth were observed over the same treatment time. All these observations further illustrate the complexity and variation in NO-mediated root development when responding to the different environmental stresses. Alternatively, increased ROS levels are also involved in excess-Fe-inhibited primary root length (Reyt *et al.*, 2015) and are the stimulus to activate NSCCs, resulting in K^+ loss from the cell (Pottosin & Dobrovinskaya, 2014; Shabala *et al.*, 2016). In agreement with the observations of Reyt *et al.* (2015), Excess Fe indeed increased ROS level in root tips of both *Col-0* and *nox1* seedlings (Fig. S12); however, the elevated ROS levels in *nox1* did not significantly differ from *Col-0* in our study, suggesting that ROS increase caused by Fe excess is not the main reason for impaired Fe resistance in the *nox1*. Meanwhile, it is important to recall that NO can increase the abundance of ferritin proteins which store Fe to avoid oxidative stress (Arnaud *et al.*, 2006; Briat *et al.*, 2010). However, Reyt *et al.* (2015) had clearly demonstrated, using genetic evidence, that ferritin is not involved in modulations of primary root growth under excess Fe. The work described in this article further shows that Fe-induced NO accumulation involved in Fe-dependent root-tip-zone K^+ homeostasis based on the pharmacological and genetic evidence.

According to the literature, effects of NO on root K^+ homeostasis can vary greatly between conditions and plant species. Chen *et al.* (2013) showed that SNP increases K^+ content under exposure to salt in *Kandelia obovata*. However, Xia *et al.* (2014) found that SNP can mediate root K^+ homeostasis by negatively regulating root potassium uptake via suppressing the AKT1 gene in *Arabidopsis*. Cd induces NO but has no effect on *Arabidopsis* root K^+ status (Besson-Bard *et al.*, 2009). These diverse results on the relationships between NO and K^+ homeostasis might be attributed to the impacts of external stimuli on NO content and different sources of NO production in plants.

Although the mechanism by which endogenous NO regulates root tip K^+ efflux under excess Fe remains to be defined, one hypothesis is that NO might influence ion channels in roots. Gd^{3+} pretreatment significantly decreased root-tip K^+ efflux in the *nox1* mutant under both control and Fe treatment (Fig. 7e,f). Recently, it was reported that enhanced NO accumulation could indirectly, via *SNO1/SOS4*, result in a reduction of K^+ uptake in the root (Xia *et al.*, 2014). Here, we provide evidence that an increase of *SNO1/SOS4* activity was observed in the excess-Fe-treated *Col-0* and *nox1* seedlings, and that the induction was more significant in *nox1* (Fig. 9a). The *SNO1/SOS4* gene is also involved in root growth and the regulation of root-tip-zone K^+ fluxes under Fe toxicity (Fig. 9b–d). It is not known at this time how the *SNO1/SOS4* gene engages to modulate root-tip K^+ efflux. Xia *et al.* (2014) demonstrated that increased *SNO1/SOS4* activity could trigger PLP accumulation and that PLP plays a critical role in regulating the *Arabidopsis* root K^+ content. PLP could stimulate root-tip K^+ efflux under excess Fe. In our study, PLP pretreatment enhanced excess-Fe-induced K^+ efflux in the *Col-0* root tip zone, and application of Gd^{3+} could reverse the PLP-induced K^+ efflux under excess Fe (Fig. 9e,f). More detailed research is warranted to examine this in the future. Interestingly, there was no significant alleviation of Fe-inhibited root growth by K^+ addition in *nox1* and *sno1/sos4* mutants, suggesting that NO might negatively regulate additional K^+ alleviation of Fe excess. One hypothesis is that overaccumulation of NO could reduce K^+ uptake (Xia *et al.*, 2014), and this might restrict the tissue K^+ concentration under K^+ addition.

Excess Fe and NO accumulation have been reported to trigger cell death (Xu *et al.*, 2010; Bai *et al.*, 2012), although the mechanism for this is not understood. Excess Fe induced ROS accumulation (Reyt *et al.*, 2015; Fig. S12), which could trigger oxidative damage and cell death (Lin *et al.*, 2012). In this study, the *nox1* mutant had more severe root-tip-cell mortality but similar ROS accumulation to *Col-0* under Fe toxicity (Fig. S12), suggesting that NO may also be involved in Fe-induced cell death. Previous reports suggested that NO induced-cell death was related to NO-mediated hormone imbalance and protein *S*-nitrosylation (Xu *et al.*, 2010; Bai *et al.*, 2012; Lin *et al.*, 2012). In addition, K^+ loss could stimulate cell death in animals and in *Arabidopsis* (Yu, 2003; Demidchik *et al.*, 2010). Consistent with this, K^+ deficiency significantly enhanced *Col-0* root-tip-zone TB-staining-indicated cell death under Fe toxicity in our study (Fig. S6d). More research is warranted to examine this.

Ethylene is regarded as a stress hormone and can be induced by a variety of stresses to protect growth, such as under salt stress (Jiang *et al.*, 2013), but ethylene accumulation in non-stressed environments can inhibit root growth (Fig. 10c) partly associated with induced hormonal imbalance (e.g. auxin, jasmonates, and abscisic acid (ABA)) (Adams & Turner, 2010; Strader *et al.*, 2010; Ma *et al.*, 2014). Ethylene has been shown to play roles in the tolerance of primary root growth to excess Fe (Peng & Yamauchi, 1993; Li *et al*., 2015b; Fig. 10), although specific mechanisms of this have remained unclear. Here, we suggest that one possible mechanism of ethylene induces tolerance in primary root growth in *Col-0* partly through NO mediation. The findings are also consistent with previous reports showing that ethylene regulates NO levels in plants (Song *et al.*, 2011; Liu *et al.*, 2017). Interestingly, treatment with the NO donor SNP could stimulate the *ACS7* gene expression in the root under Fe excess, suggesting ethylene production can respond to NO levels under Fe excess. Supportive of this are the findings by Gniazdowska *et al.* (2007) and Liu *et al.* (2017), that SNP upregulates the activities of ethylene biosynthesis enzymes.

In conclusion, NO levels in root tips are increased significantly above levels elsewhere in the root and are involved in arresting the primary root tip zone growth under excess Fe. The Fe-inhibited root growth is at least in part related to NO-induced K^+ loss, possibly via NSCCs. Meanwhile, excess Fe also affects cell viability likely via ROS accumulation and NO-induced hormone imbalance and protein *S*-nitrosylation, all of which affect root growth. These modulations in hormone and K^+ homeostasis might regulate growth rate to reduce the interceptive surface of the root system to excess Fe. Meanwhile, ethylene can partially antagonize the reduction in excess-Fe-mediated primary root growth by controlling NO levels. These compensatory effects of ethylene may prevent the excessive decline in root growth and maintain the absorption of other nutrients (Heil & Baldwin, 2002). In addition, the root hair zone is more tolerant to Fe excess and can sequestrate more Fe in the vacuole, cell wall, and by components to avoid deposition of excessive Fe in susceptible tissues (such as the root tip zone). Further research into the interplay of ion homeostasis and NO will enable a fuller understanding of how plants respond to Fe toxicity by regulating hormonal and ion signaling.

Acknowledgements

We thank Drs Caifu Jiang (China Agricultural University), Tom Guilfoyle (University of Missouri), Ben Scheres (Utrecht University) and Ningning Wang (Nankai University) for providing the seeds of *eto2-1, DR5:GUS, DR5:GFP* and *ACS7:GUS* lines, respectively, and Dr GuangQin Guo (Lanzhou University), Dr J. Alonso (North Carolina State University) and Dr Yanhua Su (Institute of Soil

Science) for providing seeds of *DR5:GUS* in *wei7-2*, *EBS:GUS* reporter lines and *gork1* mutant, respectively, and the Arabidopsis Biological Resource Centre of Ohio State University for mutant seeds. This work was supported by the National Natural Science Foundation of China (31430095), the National Key R&D Program of China (2017YFD0200103), the National Natural Science Foundation of China (31501821), the Chinese Academy of Sciences Innovation Program (CAS ISSASIP1604), and the University of Melbourne.

Author contributions

L.Z. and G.L. executed the experiments, interpreted data and generated figures, and was the major writer of the manuscript. W.S. was involved in the design of experiments, analysis and interpretation of the data, and along with G.L. was the major writer of the manuscript. H.J.K. assisted in discussion and the writing of the manuscript. M.W., D.D. and L.S. assisted in discussion. L.Z. and G.L. contributed equally to this work.

References

Adams E, Turner J. 2010. COI1, a jasmonate receptor, is involved in ethylene-induced inhibition of *Arabidopsis* root growth in the light. *Journal of Experimental Botany* **61:** 4373-4386.

Alemayehu A, Zelinová V, Bočová B, Huttová J, Mistrík I, Tamás L. 2015. Enhanced nitric oxide generation in root transition zone during the early stage of cadmium stress is required for maintaining root growth in barley. *Plant and Soil* **390:** 213-222.

Arnaud N, Murgia I, Boucherez J, Briat JF, Cellier F, Gaymard F. 2006. An iron-induced nitric oxide burst precedes ubiquitin-dependent protein degradation for *Arabidopsis AtFer1* ferritin gene expression. *Journal of Biological Chemistry* **281:** 23579-23588.

Bai S, Li M, Yao T, Wang H, Zhang Y, Xiao L, Wang J, Zhang Z, Hu Y, Liu W *et al*. 2012. Nitric oxide restrain root growth by DNA damage induced cell cycle arrest in *Arabidopsis thaliana*. *Nitric Oxide* **26:** 54-60.

Becker M, Asch F. 2005. Iron toxicity in rice-conditions and management concepts. *Journal of Plant Nutrition and Soil Science* **168:** 558-573.

Besson-Bard A, Gravot A, Richaud P, Auroy P, Duc C, Gaymard F, Taconnat L, Renou JP, Pugin A, Wendehenne D. 2009. Nitric oxide contributes to cadmium toxicity in *Arabidopsis* by promoting cadmium accumulation in roots and by up-regulating genes related to iron uptake. *Plant Physiology* **149:** 1302-1315.

Briat JF, Ravet K, Arnaud N, Duc C, Boucherez J, Touraine B, Cellier F, Gaymard F. 2010. New insights into ferritin synthesis and function highlight a link between iron homeostasis and oxidative stress in plants. *Annals of Bot*any **10:** 811-822.

Britto DT, Kronzucker HJ. 2009. Ussing's conundrum and the search for transport mechanisms in plants. *New Phytologist* **183:**243-246.

Çelik H, Asik BB, Gürel S, Katkat AV. 2010. Potassium as an intensifying factor for iron chlorosis. *International Journal of Agriculture and Biology* **12:** 359-364.

Chen J, Xiong DY, Wang WH, Hu WJ, Simon M, Xiao Q, Chen J, Liu TW, Liu X, Zheng HL. 2013. Nitric oxide mediates root K^+/Na^+ balance in a mangrove plant, *Kandelia obovata*, by enhancing the expression of AKT1-type K^+ channel and Na^+/H^+ antiporter under high salinity. *PLoS ONE* **8:** e71543.

Chen WW, Yang JL, Qin C, Jin CW, Mo JH, Ye T, Zheng SJ. 2010. Nitric oxide acts downstream of auxin to trigger root ferric-chelate reductase activity in response to iron deficiency in *Arabidopsis*. *Plant Physiology* **154:** 810-819.

Connolly EL, Guerinot ML. 2002. Iron stress in plants. *Genome Biology* **3:** 1-6.

Coskun D, Britto DT, Jean YK, Kabir I, Tolay I, Torun AA, Kronzucker HJ. 2013a. K^+ efflux and retention in response to NaCl stress do not predict salt tolerance in contrasting genotypes of rice (*Oryza sativa* L.). *PLoS ONE* **8:** e57767.

Coskun D, Britto DT, Li MY, Oh S, Kronzucker HJ. 2013b. Capacity and plasticity of potassium channels and high-affinity transporters in roots of barley and *Arabidopsis*. *Plant Physiology* **162:** 496-511.

Coskun D, Britto DT, Kronzucker HJ. 2010. Regulation and mechanism of potassium release from barley roots: an *in planta* $^{42}K^+$ analysis. *New Phytologist* **188:**1028-1038.

Crawford NM, Guo FQ. 2005. New insights into nitric oxide metabolism and regulatory functions. *Trends in Plant Science* **10:** 195-200.

Demidchik V. 2014. Mechanisms and physiological roles of K^+ efflux from root cells. *Journal of Plant Physiology* **171:** 696–707.

Demidchik V, Cuin TA, Svistunenko D, Smith SJ, Miller AJ, Shabala S, Sokolik A, Yurin V. 2010. *Arabidopsis* root K^+ efflux conductance activated by hydroxyl radicals: single-channel properties, genetic basis and involvement in stress-induced cell death. *Journal of Cell Science* **123:**1468–1479.

Demidchik V, Maathuis FJM. 2007. Physiological roles of nonselective cation channels in plants: from salt stress to signalling and development. *New Phytologist* **175:** 387–404.

Demidchik V, Shabala SN, Coutts KB, Tester MA, Davies JM. 2003. Free oxygen radicals regulate plasma membrane Ca^{2+}- and K^+-permeable channels in plant root cells. *Journal of Cell Science* **116:** 81–88.

Duan YF, Zhang WS, Li B, Wang YN, Li KX, Sodmergen, Han CY, Zhang YZ, Li X. 2010. An endoplasmic reticulum response pathway mediates programmed cell death of root tip induced by water stress in *Arabidopsis*. *New Phytologist* **186:** 681-695.

Giehl RF, Lima JE, von Wiren N. 2012. Localized iron supply triggers lateral root elongation in *Arabidopsis* by altering the AUX1-mediated auxin distribution. *The Plant Cell* **24:** 33-49.

Gniazdowska A, Dobrzynska U, Babanczyk T, Bogatek R. 2007. Breaking the apple embryo dormancy by nitric oxide involves the stimulation of ethylene production. *Planta* **225:** 1051-1057.

Graziano M, Lamattina L. 2007. Nitric oxide accumulation is required for molecular and physiological responses to iron deficiency in tomato roots. *The Plant Journal* **52:** 949-960.

Gupta KJ, Fernie AR, Kaiser WM, van Dongen JT. 2011. On the origins of nitric oxide. *Trends in Plant Science* **16:** 1360-1385

Heil M, Baldwin IT. 2002. Fitness costs of induced resistance: emerging experimental support for a slippery concept. *Trends in Plant Science* **7:** 61–67.

Jiang CF, Belfield EJ, Cao Y, Smith YAJ, Harberd NP. 2013. An *Arabidopsis* soil-salinity-tolerance mutation confers ethylene-mediated enhancement of sodium/potassium homeostasis. *The Plant Cell* **25:** 3535-3552.

Jones DL, Kochian LV. 1995. Aluminum inhibition of the 1,4,5-trisphosphate signal transduction pathway in wheat roots: a role in aluminum toxicity? *The Plant Cell* **7:** 1913-1922.

Kronzucker HJ, Britto DT. 2011. Sodium transport in plants: a critical review**.** *New Phytologist* **189:** 54-81.

Kronzucker HJ, Szczerba MW, Schulze LM, Britto DT. 2008. Non-reciprocal interactions between K^+ and Na^+ ions in barley (*Hordeum vulgare* L.). *Journal of Experimental Botany* **59:** 2793-2801.

Li BH, Li GJ, Kronzucker HJ, Baluska F, Weiming Shi. **2014.** Ammonium stress in Arabidopsis: signaling, genetic loci, and physiological targets. *Trends in Plant Science* **19:** 107-114.

Li GJ, Kronzucker HJ, Shi WM. 2016a. Root developmental adaptation to Fe toxicity: mechanisms and management. *Plant Signaling & Behavior* **11:** e1117722.

Li GJ, Kronzucker HJ, Shi WM. 2016b. The response of the root apex in plant adaptation to iron heterogeneity in soil. *Frontiers in Plant Science* **7:** 344.

Li GJ, Li BH, Dong GQ, Feng XY, Kronzucker HJ, Shi WM. 2013. Ammonium-induced shoot ethylene production is associated with the inhibition of lateral root formation in *Arabidopsis*. *Journal of Experimental Botany* **64:** 1413-1425.

Li GJ, Song HY, Li BH, Kronzucker HJ, Shi WM. 2015a. Auxin resistant1 and PIN-FORMED2 protect lateral root formation in *Arabidopsis* under iron stress. *Plant Physiology* **169:** 2608-2623.

Li GJ, Xu WF, Kronzucker HJ, Shi WM. 2015b. Ethylene is critical to the maintenance of primary root growth and Fe homeostasis under Fe stress in *Arabidopsis*. *Journal of Experimental Botany* **66:** 2041-2054.

Li H, Yang X, Luo AC. 2001. Ameliorating effect of potassium on iron toxicity in hybrid rice. *Journal of Plant Nutrition* **24:** 1849-60.

Li Q, Li BH, Kronzucker HJ, Shi WM. 2010. Root growth inhibition by NH_4^+ in *Arabidopsis* is mediated by the root tip and is linked to NH_4^+ efflux and GMPase activity. *Plant, Cell & Environment* **33:** 1529-1542.

Li XN, Ma HZ, Jia PX, Wang J, Jia LY, Zhang TG, Yang YL, Chen HJ, Wei X. 2012. Responses of seedling growth and antioxidant activity to excess iron and copper in *Triticum aestivum* L. *Ecotoxicology and Environmental Safety* **86:** 47-53.

Lin AH, Wang YQ, Tang JY, Xue P, Li CL, Liu LC, Hu B, Yang FQ, Loake GJ, Chu CC. 2012. Nitric oxide and protein S-nitrosylation are integral to hydrogen peroxide-induced leaf cell death in rice. *Plant Physiology* **158:** 451-464.

Liu ML, Liu XX, He XL, Liu LJ, Wu H, Tang CX, Zhang YS, Jin CW. 2017. Ethylene and nitric oxide interact to regulate the magnesium deficiency-induced root hair development in *Arabidopsis*. *New Phytologist* **213:** 1242-1256.

Liu SL, Yang RJ, Pan YZ, Ren B, Chen QB, Li X, Xiong X, Tao JJ, Cheng QS, Ma MD. 2016. Beneficial behavior of nitric oxide in copper-treated medicinal plants. *Journal of Hazardous Materials* **314:** 140-154.

Liu W, Li RJ, Han TT, Cai W, Fu ZW, Lu YT. 2015. Salt stress reduces root meristem size by nitric oxide mediated modulation of auxin accumulation and signaling in *Arabidopsis*. *Plant Physiology* **168:** 343-356.

Ludewig U, Wilken S, Wu B, Jost W, Obrdlik P, El Bakkoury M, Marini AM, Andre B, Hamacher T, Boles E *et al.* 2003. Homo-and hetero-oligomerization of ammonium transporter-1 NH_4^+ uniporters. *Journal of Biological Chemistry* **278:** 45603-45610.

Luxova M. 1988. The participation of the primary maize root on the assimilation of NH_4^+ ions. *Plant and Soil* **111:** 187–189.

Ma B, Yin CC, He SJ, Lu X, Zhang WK Lu TG, Chen SY, Zhang JS. 2014. Ethylene-induced inhibition of root growth requires abscisic acid function in Rice (*Oryza sativa* L.) seedlings. *PLoS Genetics* **10:** e1004701.

Meguro R, Asano Y, Odagiri S, Li C, Iwatsuki H, Shoumura K. 2007. Nonheme-iron histochemistry for light and electron microscopy: a historical, theoretical and technical review. *Archive of Histology and Cytology* **70:** 1-19.

Muller J, Toev T, Heisters M, Teller J, Moore KL, Hause G, Dinesh DC, Burstenbinder K, Abel S. 2015. Iron-dependent callose deposition adjusts root meristem maintenance to phosphate availability. *Developmental Cell* **33:** 216-230.

Neill SJ, Desikan R, Hancock JT. 2003. Nitric oxide signalling in plants. *New Phytologist* **159:** 11-35.

Onaga G, Dramé KN, M. Ismail A. 2016. Understanding the regulation of iron nutrition: can it contribute to improving iron toxicity tolerance in rice? *Functional Plant Biology* **43:** 709-726

Pagnussat G.C, Simontacchi M, Puntarulo S, Lamattina L. 2002. Nitric oxide is required for root organogenesis. *Plant Physiology* **129:** 954-956.

Peng XX, Yamauchi M. 1993. Ethylene production in rice bronzing leaves induced by ferrous iron. *Plant and Soil* **149:** 227-234.

Peto A, Lehotai N, Feigl G, Tugyi N, Ordog A, Gemes K, Tari I, Erdei L, Kolbert Z. 2013. Nitric oxide contributes to copper tolerance by influencing ROS metabolism in *Arabidopsis*. *Plant Cell Report* **32:** 1913-1923.

Pottosin I, Dobrovinskaya O. 2014. Non-selective cation channels in plasma and vacuolar membranes and their contribution to K^+ transport. *Journal of Plant Physiology* **171:** 732–742.

Reyt G, Boudouf S, Boucherez J, Gaymard F, Briat JF. 2015. Iron and ferritin dependent ROS distribution impact *Arabidopsis* root system architecture. *Molecular Plant* **8:** 439-453.

Roschzttardtz H, Conejero G, Curie C, Mari S. 2009. Identification of the endodermal vacuole as the iron storage compartment in the *Arabidopsis* embryo. *Plant Physiology* **151:** 1329-1338.

Shabala S, Demidchik V, Shabala L, Cuin TA, Smith SJ, Miller AJ, Davies JM, Newman IA. 2006. Extracellular Ca^{2+} ameliorates NaCl-induced K^+ loss from *Arabidopsis* root and leaf cells by controlling plasma membrane K^+-permeable channels. *Plant Physiology* **141:** 1653–1665.

Shabala L, Zhang JY, Pottosin I, Bose J, Zhu M, Fuglsang AT, Velarde-Buendia A, Massart A, Hill CB, Roessner U *et al*. 2016. Cell-type-specific H^+-ATPase activity in root tissues enables K^+ retention and mediates acclimation of Barley (*Hordeum vulgare*) to salinity stress. *Plant Physiology* **172:** 2445-2458.

Shi HZ, Xiong LM, Stevenson B, Lu T, Zhu JK. 2002. The Arabidopsis *salt overly sensitive 4* mutants uncover a critical role for vitamin B6 in plant salt tolerance. *The Plant Cell* **14:** 575-588.

Simontacchi M, Galatro A, Ramos-Artuso FE. Santa-María G. 2015. Plant survival in a changing environment: the role of nitric oxide in plant responses to abiotic stress. *Frontiers in Plant Science* **6:** 977.

Song XG, She XP, Wang J, Sun YC. 2011. Ethylene inhibits darkness-induced stomatal closure by scavenging nitric oxide in guard cells of *Vicia faba*. *Functional Plant Biology* **38:** 767-777.

Sun CL, Lu LL, Liu LJ, Liu WJ, Yu Y, Liu XX, Hu Y, Jin CW, Lin XY. 2014. Nitrate reductase-mediated early nitric oxide burst alleviates oxidative damage induced by aluminum through enhancement of antioxidant defenses in roots of wheat (*Triticum aestivum*). *New Phytologist* **201:** 1240-1250.

Strader LC, Chen GL, Bartel B. 2010. Ethylene directs auxin to control root cell expansion. *The Plant Journal* **64:** 874–884.

Szczerba MW, Britto DT, Kronzucker HJ. 2009. K^+ transport in plants: physiology and molecular biology. *Journal of Plant Physiology* **166:** 447-466.

Teerawanichpan P, Hoffman T, Ashe P, Datla R, Selvarai G. 2007. Investigations of combinations of mutations in the jellyfish green fluorescent protein (GFP) that afford brighter fluorescence, and use of a version (VisGreen) in plant, bacterial, and animal cells. *Biochimica et Biophysica Acta* **1770:** 1360–1368.

Tian QY, Sun DH, Zhao MG, Zhang WH. 2007. Inhibition of nitric oxide synthase (NOS) underlies aluminum-induced inhibition of root elongation in *Hibiscus moscheutos*. *New Phytologist* **174:** 322-331.

Touraine B, Briat JF, Gaymard F. 2012. GSH threshold requirement for NO-mediated expression of the *Arabidopsis* AtFer1 ferritin gene in response to iron. *FEBS Letters* **586:** 880-883.

Tsukagoshi H, Busch W, Benfey PN. 2010. Transcriptional regulation of ROS controls transition from proliferation to differentiation in the root. *Cell* **143:** 606-616.

Wang F, Chen ZH, Liu X, Colmer TD, Zhou M, Shabala S. 2016. Tissue-specific root ion profiling reveals essential roles for the CAX and ACA calcium transport systems for hypoxia response in *Arabidopsis*. *Journal of Experimental Botany* **67:** 3747-3762.

Wang KLC, Yoshida H, Lurin C, Ecker JR. 2004. Regulation of ethylene gas biosynthesis by the *Arabidopsis* ETO1 protein. *Nature* **428:** 945-950.

Wang L, Guo YJ, Jia LX, Chu HY, Cheng KM, Wu D, Zhao LQ. 2014. Hydrogen peroxide acts upstream of nitric oxide in the heat shock pathway in *Arabidopsis* seedlings. *Plant Physiology* **164:** 2184-2196.

Ward JT, Lahner B, Yakubova E, Salt DE, Raghothama KG. 2008. The effect of iron on the primary root elongation of *Arabidopsis* during phosphate deficiency. *Plant Physiology* **147:** 1181-1191.

Weigel D, Glazebrook J. 2002. How to study gene expression. In: Weigel D, Glazebrook J, eds. Arabidopsis: *a laboratory manual*. New York, NY, USA: Cold Spring Harbor Laboratory Press, 243-245.

Wheeler BD, Al-Farraj MM, Cook RED. 1985. Iron toxicity to plants in base-rich wetlands:

comparative effects on the distribution and growth of *Epilobium Hirsutum* L. and *Funcus subnodulosus schrank*. *New Phytologist* **100:** 653-669.

Xia J, Kong D, Xue S, Tian W, Li N, Bao F, Hu Y, Du J, Wang Y, Pan XJ, Wang L *et al*. 2014. Nitric oxide negatively regulates AKT1-mediatedpotassium uptake through modulating vitamin B6 homeostasis in *Arabidopsis*. *Proceedings of the National Academy of Sciences, USA* **111:** 16196-16201.

Xiong J, Fu G, Tao L, Zhu C. 2010. Roles of nitric oxide in alleviating heavy metal toxicity in plants. *Archives of Biochemistry and Biophysics* **497:** 13-20.

Xu J, Yin HX, Li YL, Liu XJ. 2010. Nitric oxide is associated with long-term zinc tolerance in *Solanum nigrum*. *Plant Physiology* **154:** 1319-1334.

Yang ZB, Geng X, He C, Zhang F, Wang R, Horst WJ Ding ZJ. 2014. TAA1-regulated local auxin biosynthesis in the root-apex transition zone mediates the aluminum-induced inhibition of root growth in *Arabidopsis*. *The Plant Cell* **26:** 2889-2904.

Yu SP. 2003. Regulation and critical role of potassium homeostasis in apoptosis. *Progress in Neurobiology* **70:** 363-386.

Yuan HM, Huang X. 2016. Inhibition of root meristem growth by cadmium involves nitric oxide-mediated repression of auxin accumulation and signalling in *Arabidopsis*. *Plant, Cell & Environment* **39:** 120-135.

Yuan HM, Xu HH, Liu WC, Lu YT. 2013. Copper regulates primary root elongation through PIN1-mediated auxin redistribution. *Plant Cell & Physiology* **54:** 766-778.

Zepeda-Jazo I, Velarde-Buendía AM, Enríquez-Figueroa R, Bose J, Shabala S, MunizMurguía J, Pottosin I. 2011. Polyamines interact with hydroxyl radicals in activating Ca^{2+} and K^+ transport across the root epidermal plasma membranes. *Plant Physiology* **157:** 2167–2180.

Zhang Y, Wang YP, Liu P, Song JM, Xu GD, Zheng GH. 2012. Effect of toxic Fe^{2+} level on the biological characteristics of rice root border cell. *Russian Journal of Plant Physiology* **59:** 766-771.

Zhang Y, Zheng GH, Liu P, Song JM, Xu GD, Cai MZ. 2011. Morphological and physiological responses of root tip cells to Fe^{2+} toxicity in rice. *Acta Physiologiae Plantrum* **33:** 683-689.

Zhou Y, Xu XY, Chen LQ, Yang JL, Zheng SJ. 2012. Nitric oxide exacerbates Al-induced inhibition of root elongation in rice bean by affecting cell wall and plasma membrane properties. *Phytochemistry* **76:** 46-51.

Supporting Information

Additional Supporting Information may be found online in the Supporting Information tab for this article:

Fig. S1 Schematic diagram of the experimental setup for applying excess Fe to the root tip zone.

Fig. S2 Effects of excess Fe on root Fe staining (Perls staining) in control and in seedlings treated with excess Fe.

Fig. S3 Effects of localized low-K^+ supply on root growth of *Arabidopsis*.

Fig. S4 Effects of excess Fe on root-tip-zone Na, Ca and Mg level in *Arabidopsis*.

Fig. S5 Effects of Gd^{3+} on the Fe-inhibited root growth and effects of excess Fe on the root growth of *gork1* mutants.

Fig. S6 Effects of the K^+ on the root growth, net plasma-membrane K^+ fluxes, K content and cell viability in the root tip zone under Fe excess.

Fig. S7 Effects of L-NAME and L-NMME on primary root growth of *Arabidopsis*.

Fig. S8 Effects of excess Fe on primary root growth in *Arabidopsis Col-0* and *gsnor1* mutant.

Fig. S9 Effects of Fe-citrate and K-citrate on primary root growth in *Arabidopsis Col-0* and *nox1* mutant.

Fig. S10 Effects of Cu stress on root growth of *Col-0* and *nox1*.

Fig. S11 Effects of auxin on excess Fe-mediated primary root growth inhibition in *Arabidopsis*.

Fig. S12 Effects of excess Fe on the production of ROS in roots of *Arabidopsis Col-0* and *nox1* plants.

Fig. S13 Effects of NO on net plasma-membrane K^+ fluxes in the root tip zone under control conditions.

Fig. S14 Effects Gd^{3+} on the NO level of *Col-0* root tip zone.

Fig. S15 Effects of excess Fe on the cell death of *Col-0* and *nox1* root tip zone.

Fig. S16 Effects of the NO on K^+ alleviation of primary root growth inhibition under excess Fe.

Fig. S17 Effects of excess Fe on activity of *EBS:GUS* in *Arabidopsis* root tissue.

Fig. S18 Effects of the NO donor SNP on the activity of *AtACS7:GUS* in *Arabidopsis* root tissue.

Table S1 Genetic loci of the *Arabidopsis thaliana* mutants used in this study

Please note: Wiley Blackwell are not responsible for the content or functionality of any supporting information supplied by the authors. Any queries (other than missing material) should be directed to the *New Phytologist* Central Office.

Fig. 1 Effects of excess iron (Fe) on primary root growth in *Arabidopsis thaliana* (*Col-0*). (a)

Primary root growth of 5-d-old *Col-0* exposed to serial concentrations of Fe-EDTA for 5 d. (b) Root growth rate as a function of time after treatment. Ctrl, control, 50 μM Fe; +Fe, excess Fe, 300 μM Fe. (c) The effect of locally supplied Fe on root growth rate as a function of time after treatment. Values shown are means ± SD ($n \geq 14$). Asterisks indicate statistical differences between control (Ctrl) and excess Fe treatment (+Fe) (independent samples *t*-test, $P < 0.05$).

Fig. 2 Effects of excess iron (Fe) on root Fe and potassium (K) homeostasis in control and excess-Fe-treated *Arabidopsis thaliana* (*Col-0*) seedlings. (a) Distance from the root apex to the first root hair of the primary root. Photographs show representative seedlings treated for 3 d. Black arrows indicate the position of the first root hair. (b) The quantification of distance from the root apex to the first root hair. Asterisk denotes statistical significance (independent samples *t*-test, $n = 20–21$, $P < 0.05$). (c) Fe accumulation and distribution in primary roots. Five-day-old *Col-0* seedlings exposed to excess Fe for 3 d before Perls/diaminobenzidine (DAB) staining. (d) Effect of excess Fe on K^+ staining in the *Arabidopsis* root hair zone and tip zone. Five-day-old *Col-0* seedlings exposed to excess Fe for 3 d before stain with K^+ indicator (Asante Potassium Green-2, APG-2). (e) The mean relative APG-2 fluorescence intensity in the root tip (RT) and root hair zone (RHZ) of control and excess-Fe-treated seedlings. The fluorescence intensity of control root tip and hair zone was set to 1. Asterisk denotes statistical significance (independent samples *t*-test, $n = 12$, $P < 0.05$). (f) Effect of Fe excess on K content in the root tip zone. Five-day-old *Col-0* seedlings were transferred for 3 d to control or excess Fe before harvesting root tips (*c*. 1–2 mm) for ICP-MS measurements of K (values shown are the means ± SD of three replicates, each with three biological replicates of *c*. 100 root tips each, asterisk denotes statistical significance). Bars: (a) 500 μm; (c, d) 100 μm.

Fig. 3 Influence of excess Fe on net plasma membrane K^+ fluxes of *Arabidopsis thaliana* (*Col-0*). (a) Net K^+ fluxes measured from the epidermal root cells in the root apical (*c*. 500 μm from the tip) transition zone and root hair (*c*. 3000 μm from the tip) zones of *Col-0* seedlings in response to 300 μM Fe treatment (indicated by the arrow). (b) Mean values of K^+ fluxes from (a). Asterisk denotes statistical significance (independent samples *t*-test, $P < 0.05$). (c) The effect of locally supplied Fe on net K^+ fluxes in the root tip zone (indicated by the arrow). (d) Mean values of K^+ fluxes from (c). Asterisk denotes statistical significance (independent samples *t*-test, $P < 0.05$; ns, nonsignificant). Values shown are the means ± SD ($n \geq 3$). Whole + Fe, the whole seedlings supplied excess Fe.

Fig. 4 The effect of excess Fe on net plasma-membrane K^+ efflux in the root tip zone of *Arabidopsis thaliana Col-0* with or without tetraethylammonium (TEA), Gd^{3+} pretreatment, and in the *gork1* mutant. (a) Effect of TEA (10 mM) and Gd^{3+} (50 μM) pretreatment on net K^+ fluxes measured from the epidermal root cells in the *Col-0* root apical zone in response to 300 μM Fe treatment (indicated by the arrow). (b) Mean values of K^+ fluxes from (a). Asterisk denotes statistical significance (independent samples *t*-test, $n \geq 3$, $P < 0.05$; ns, nonsignificant). (c) The net K^+ fluxes measured from the epidermal root cells in the *Wassilewskija* (WS) and *gork1* root apical zone in response to 300 μM Fe treatment (indicated by the arrow). (d) Mean values of K^+ fluxes from (c). Asterisk denotes statistical significance (independent samples *t*-test, $n = 8$, $P < 0.05$; ns, nonsignificant). Values shown are the means ± SD.

Fig. 5 Effects of excess Fe on the production of nitric oxide (NO) in roots of *Arabidopsis thaliana Col-0* plants. 5-d-old *Col-0* seedlings exposed to excess Fe for 2 d. (a) The endogenous NO level in root tip zone and root hair zone was monitored by labeling NO using the NO-specific fluorescent probe DAF-FM DA and imaged by epifluorescence microscopy. Bars, 100 μm. (b) The mean relative DAF-FM fluorescence intensity in the root tip (RT) and root hair zone (RHZ) of control and excess-Fe-treated seedlings. The fluorescence intensity of control root tip zone was set to 1. Values shown are the means ± SD ($n = 15$). Different letters represent means that are statistically different at the 0.05 level (one-way ANOVA with Duncan post hoc test). Ctrl, control (50 μM Fe); +Fe, excess Fe (300 μM Fe).

Fig. 6 Effects of nitric oxide (NO) on excess Fe-mediated primary root growth in *Arabidopsis thaliana*. (a) Effect of NO scavenger 2-(4-carboxyphenyl)-4,4,5,5-tetramethylimidazoline-1-oxyl-3-oxide (cPTIO) (100 μM) on primary root growth of *Col-0* seedlings grown in control (Ctrl) and 300 μM Fe (+Fe) medium. Five-day-old *Col-0* seedlings exposed to excess Fe for 5 d. (b) Distance from the root apex to the first root hair of the primary root. Asterisk indicate statistical differences between the mock and treatment under excess Fe (independent samples *t*-test, $P < 0.05$). (c) Effect of the NO donor sodium nitroprusside (SNP) (15 μM) on primary root growth of the *Col-0* seedlings. Five-day-old *Col-0* exposed to excess Fe for 3 d. (d) Effect of excess Fe on primary root growth in *Col-0* and the NO-overproduction mutant *nox1*. *Col-0* and *nox1* seedlings exposed to excess Fe for 5 d. (e) The effect of locally supplied Fe on root growth of the *Col-0* and *nox1*. *Col-0* and *nox1* seedlings exposed to excess Fe for 3 d. (f) Distance from the root apex to the first root hair of the primary root. Values shown are the means ± SD ($n \geq 10$). Different letters represent means that are statistically different at the 0.05 level (one-way ANOVA with Duncan post hoc test).

Fig. 7 Effects of nitric oxide (NO) on excess Fe-mediated net plasma-membrane K^+ fluxes in the *Arabidopsis thaliana* root tip zone. (a) Effect of 2-(4-carboxyphenyl)-4,4,5,5-tetramethylimidazoline-1-oxyl-3-oxide (cPTIO) (100 μM) and sodium nitroprusside (SNP) (15 μM) pretreatment on net K^+ fluxes from epidermal root cells in the *Col-0* root apical zone in response to 300 μM Fe (indicated by the arrow). (b) Mean values of K^+ fluxes from (a). Asterisk denotes statistical significance ($n \geq 3$, independent samples *t*-test, $P < 0.05$). (c) Effects of excess Fe on net K^+ fluxes at the root apical transition zone of the *Col-0* and the *nox1* mutant. (d) Mean values of K^+ fluxes from (c). Asterisk denotes statistical significance. (e) Effect of Gd^{3+} (50 μM) pretreatment on net K^+ fluxes from epidermal root cells in the *nox1* root apical zone in response to 300 μM Fe. (f) Mean values of K^+ fluxes from (e). Asterisks denote statistical significance ($n \geq 3$, independent samples *t*-test, $P < 0.05$). Values shown are the means ± SD.

Fig. 8 Effect of excess Fe on Asante Potassium Green-2 (APG-2) staining in the *Arabidopsis thaliana Col-0* and *nox1* root tip zone. Five-day-old seedlings exposed to excess Fe for 3 d before staining with a K^+ indicator (APG-2). Bar, 100 μm. The quantification of samples is shown in the images, and the fluorescence intensity of *Col-0* control root tip zone was set to 1. Asterisks denote statistical significance compared with *Col-0* control (independent samples *t*-test, $P<0.05$). Values shown are the means ± SD (n =10–12).

Fig. 9 Effects of SNO1/SOS4 on the Fe-mediated root growth and net plasma-membrane K^+ fluxes in the *Arabidopsis thaliana* root tip zone. (a) Enzyme activity of SNO1/SOS4 in *Col-0* and *nox1* roots in response to sodium nitroprusside (SNP) (15 μM) and excess Fe (300 μM). Seven-day-old seedlings exposed to excess Fe for 3 d. Different letters represent means that are statistically different at the 0.05 level (one-way ANOVA with Duncan post hoc test). (b) Effect of excess Fe on primary root growth in the *Col-0* and the *sno1/sos4* mutant. Five-day-old seedlings exposed to excess Fe for 5 d. Different letters represent means that are statistically different at the 0.05 level (one-way ANOVA with Duncan post hoc test) (n = 10). (c) Effects of excess Fe (indicated by the arrow) on net K^+ fluxes at the root apical transition zone of *Col-0* and *sno1/sos4* mutant seedlings. (d) Mean values of K^+ fluxes from (c). Asterisk denotes statistical significance ($n \geq 3$, independent samples *t*-test, $P < 0.05$). (e) Effect of pyridoxal-5'-phosphate (PLP) (100 μM) and PLP plus Gd^{3+} (50 μM) pretreatment on net K^+ fluxes from epidermal root cells in the *Col-0* root apical zone in response to 300 μM Fe (indicated by the arrow). (f) Mean values of K^+ fluxes under excess Fe from (e). Asterisk denotes statistical significance ($n \geq 4$, independent samples *t*-test, $P < 0.05$; ns, nonsignificant **[Author, please confirm inserted text 'ns, nonsignificant' is correct]**). Values shown are the means ± SD.

Fig. 10 Effects of ethylene on Fe-mediated root growth, nitric oxide (NO) production, and net plasma-membrane K^+ fluxes in the *Arabidopsis thaliana* root-tip zone. (a) Activity of *AtACS7:GUS* (ACC synthase, ACS) in *Arabidopsis* root tissue. Five-day-old seedlings exposed to excess Fe for 2 d. One representative sample from each treatment (seven plants) is shown. (b) Effect of the ethylene inhibitor aminoethoxyvinylglycine (AVG) (0.75 μM) on primary root growth of *Col-0* seedlings grown in control and Fe treatment media. Five-day-old seedlings exposed to excess Fe for 3 d. (c) Effect of excess Fe on primary root growth in *Col-0* seedlings and the ethylene-overproducing mutant *eto2-1*. (d) Effect of the ethylene inhibitor AVG (0.75 μM) on NO production in the root tip zone. Five-day-old seedlings exposed to excess Fe for 2 d. One representative sample from each treatment (n = 14–15) is shown, and the fluorescence intensity of control mock root tip zone was set to 1. (e) Effects of excess Fe on the production of NO in roots of *Arabidopsis Col-0* and *eto2-1* plants. Five-day-old seedlings exposed to excess Fe for 2 d. One representative sample from each treatment (n = 11–12) is shown, and the fluorescence intensity of *Col-0* root tip zone was set to 1. (f) Effect of AVG (0.75 μM) pretreatment on net K^+ fluxes from epidermal root cells in the root apical zone in response to 300 μM Fe (indicated by the arrow). (g) Mean values of K^+ fluxes from (f). Asterisk denotes statistical significance (independent samples *t*-test, $P < 0.05$). Values shown are the means ± SD ($n \geq 3$). Different letters represent means statistically different at the 0.05 level (one-way ANOVA with Duncan post hoc test). Ctrl, control (50 μM Fe); +Fe, excess Fe (300 μM Fe). Bars, 100 μm.

Fig. 11 A proposed model for nitric oxide (NO)-mediated *Arabidopsis thaliana* primary root-tip-zone growth in *Arabidopsis* under iron (Fe) excess. NO levels in root tips are increased significantly above levels elsewhere in the root and are involved in arresting the primary root-tip-zone growth under excess Fe. NO-mediated inhibition of root growth is at least in part related to NO-induced K^+ loss, via nonselective cation channels (NSCCs), and increased *SNO1* (*sensitive to nitric oxide 1*)/*SOS4* (*salt overly sensitive 4*)-activity-mediated pyridoxal-5’-phosphate (PLP) is further implicated in this process. NO also mediates K^+ homeostasis by negatively regulating K^+ uptake. The significant K^+ loss can result in the loss of cell turgor (and, hence, arrest root growth) and either programmed cell death (PCD) or necrosis in the root apex. Meanwhile, excess Fe also reduces cell viability, associated with reactive oxygen species (ROS) accumulation and NO-induced hormone imbalance and protein *S*-nitrosylation. ROS has also been reported to activate NSCCs, resulting in K^+ loss from the cell. Furthermore, Fe-induced ethylene can partially antagonize the reduction in excess-Fe-mediated primary root growth by controlling NO levels. GORK1, guard cell outward-rectifying K^+ channel 1.

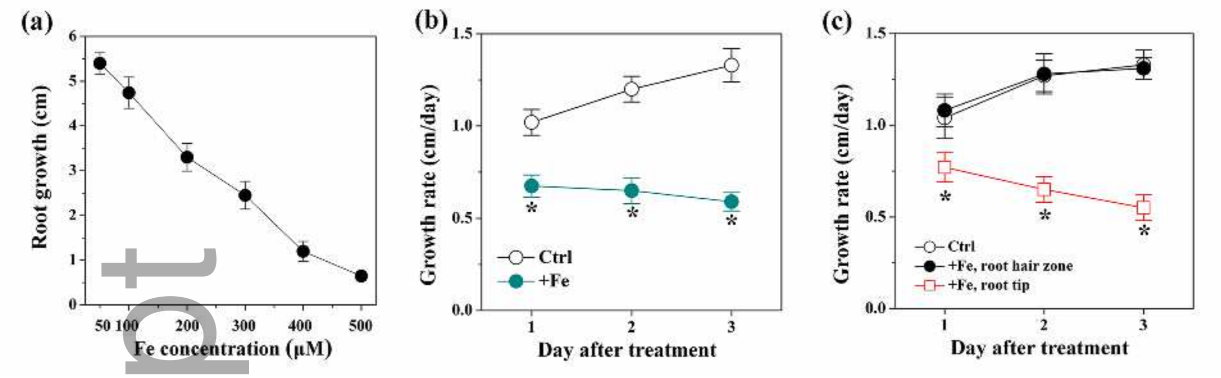

nph_15157_f1.tif

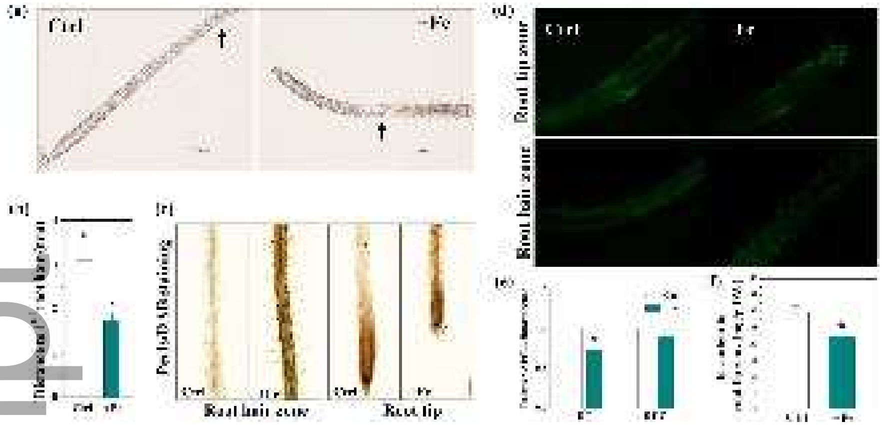

nph_15157_f2.tif

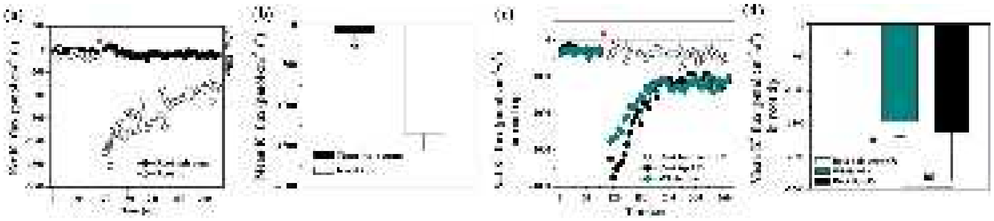

nph_15157_f3.tif

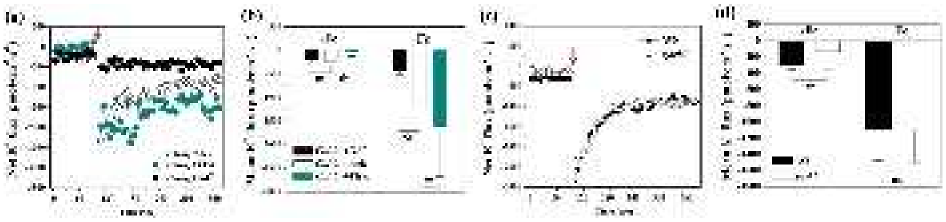

nph_15157_f4.tif

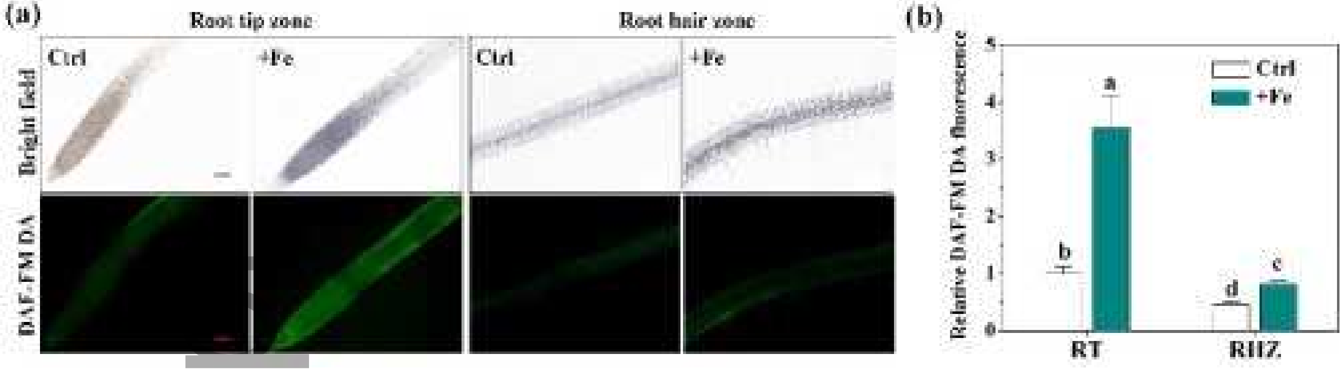

nph_15157_f5.tif

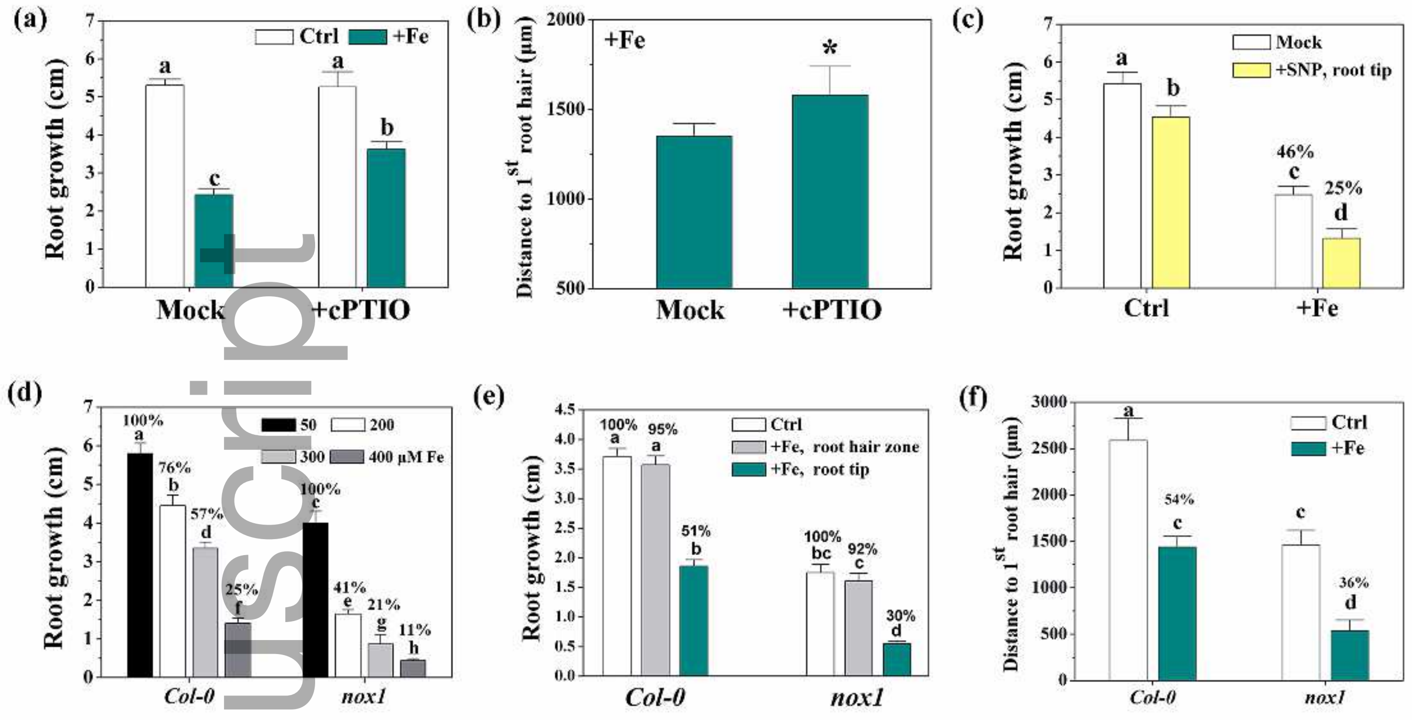

nph_15157_f6.tif

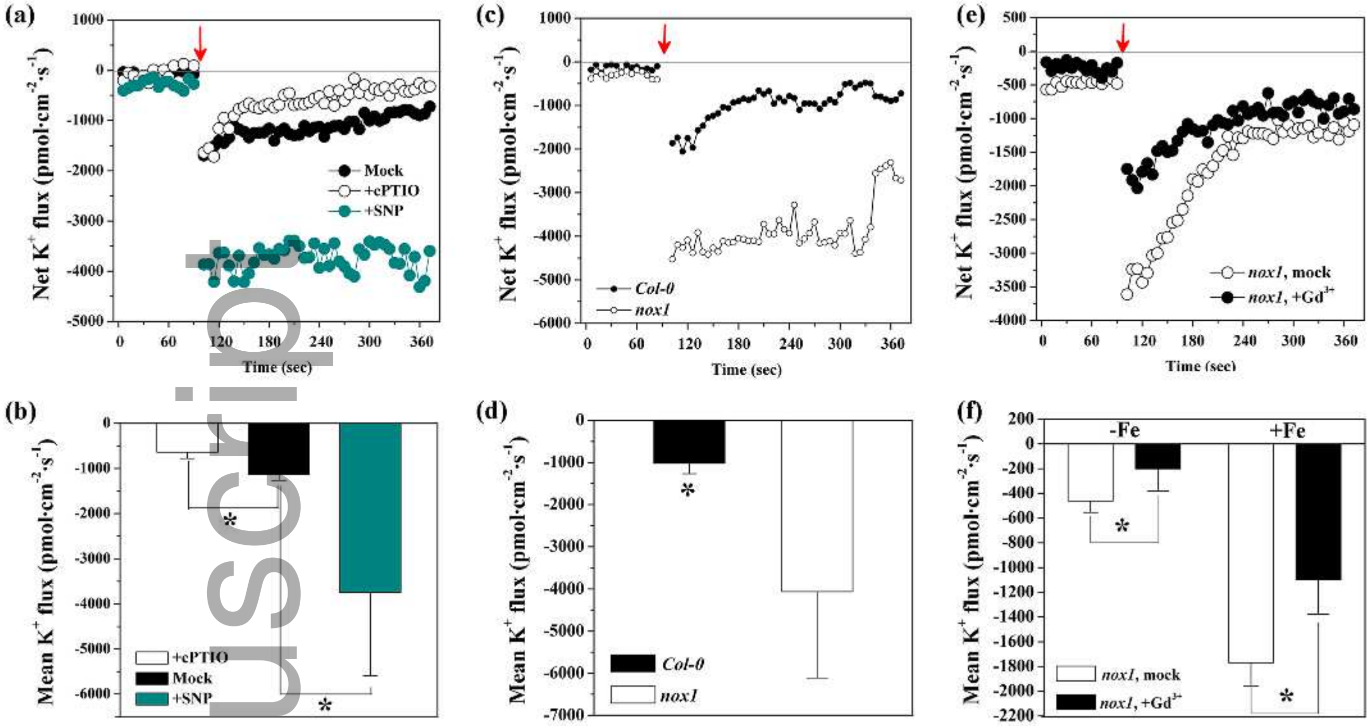

nph_15157_f7.tif

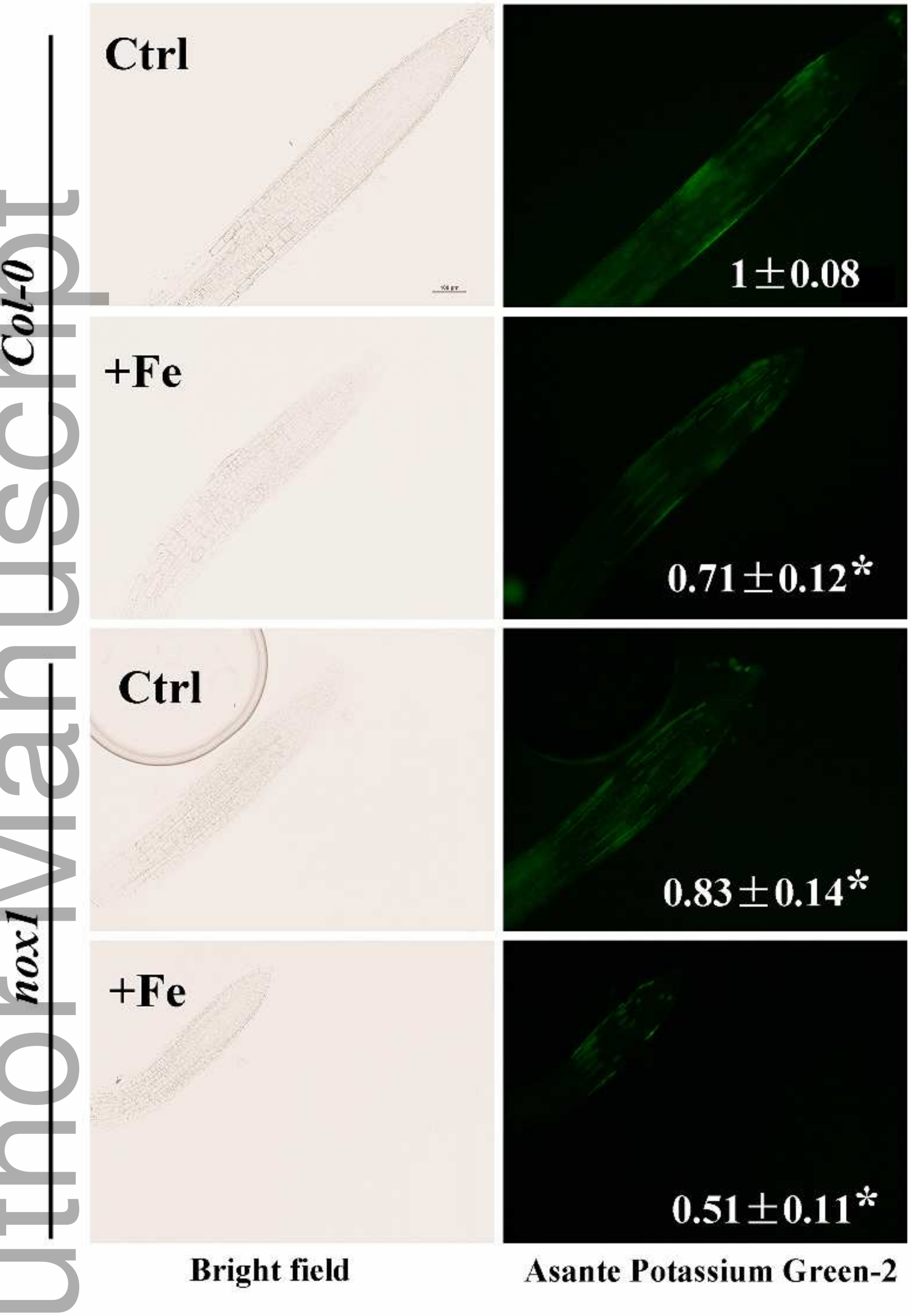

nph_15157_f8.tif

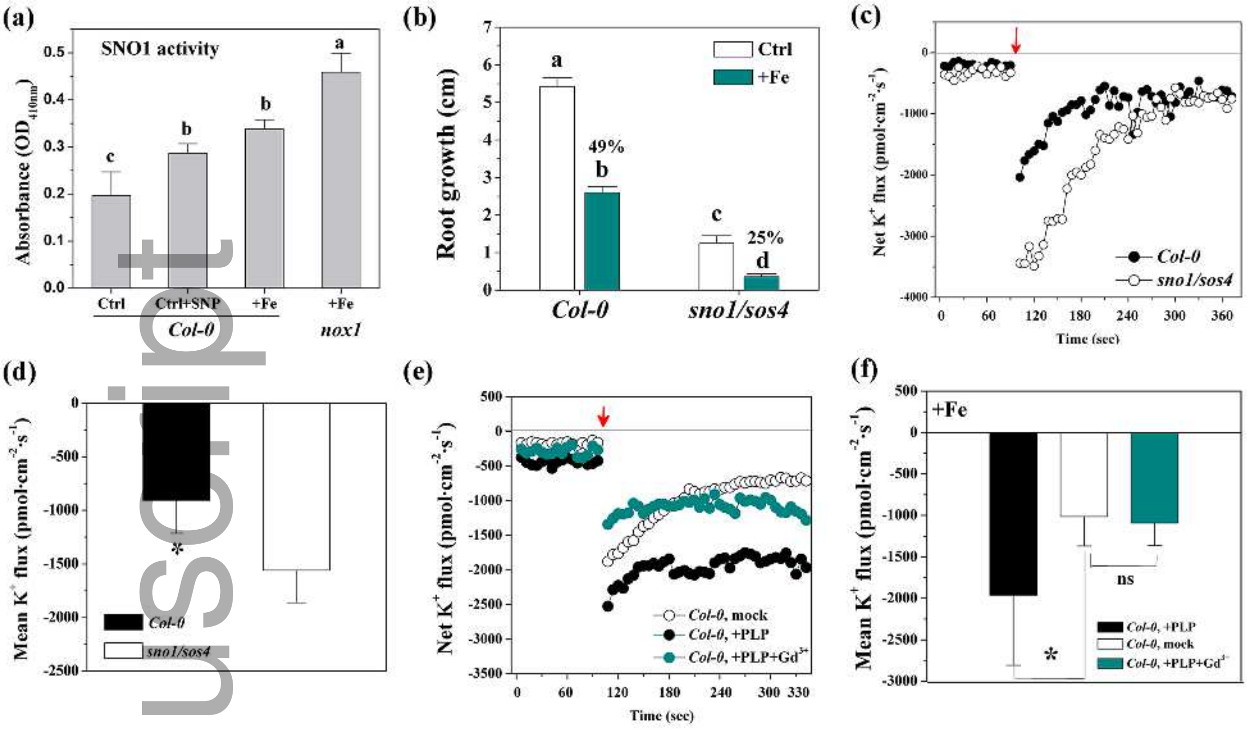

nph_15157_f9.tif

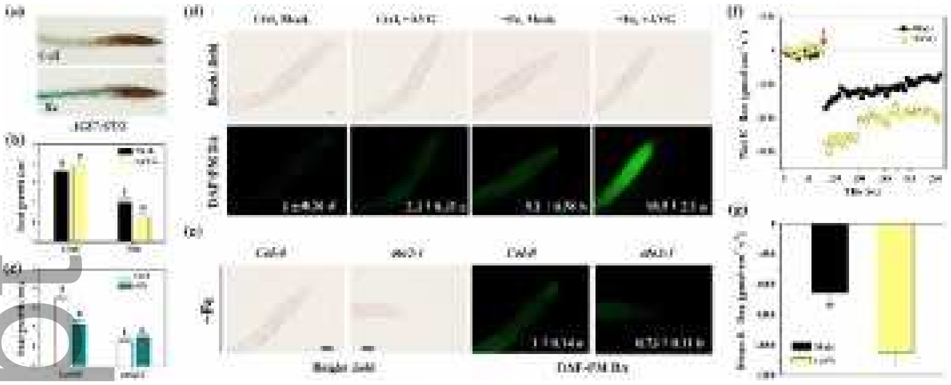

nph_15157_f10.tif

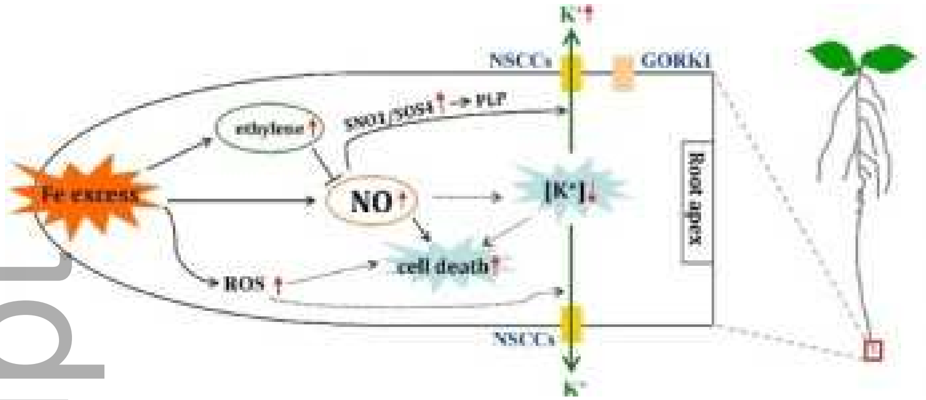

nph_15157_f11.tif